Full Paper Wiley Online Library ELECTROANALYSIS

DOI: 10.1002/elan.201600085

Reduced Graphene Oxide Non-covalent Functionalized with Zinc Tetra Phenyl Porphyrin Nanocomposite for Electrochemical Detection of Dopamine in Human Serum and Rat Brain Samples

Subramanian Sakthinathan,[a] Subbiramaniyan Kubendhiran,[a] Shen Ming Chen,*[a] Kesavan Manibalan,[a] Mani Govindasamy,[a] P. Tamizhdurai,[b] and Sheng Tung Huang*[a]

Abstract: We described the use of a nanocomposite consisting of reduced graphene oxide and zinc tetraphenylporphyrin (RGO/Zn-TPP) for electrochemical sensing of dopamine (DA). The surface of RGO was homogeneously functionalized with Zn-TPP via non-covalent π-π interaction. The nanocomposite was characterized by scanning electron microscopy, UV-Vis spectrometry, nuclear magnetic resonance spectroscopy and electrochemical impedance spectroscopy. The electroanalysis behavior of the nanocomposite was studied by cyclic voltammetry and amperometry. The excellent electrocatalytic activity is found for oxidation of DA, best at working voltage of 0.214 V (vs. Ag/AgCl) and linear response range of 0.04–238.8 μM. The sensitivity and detection limit were of 0.665 $\mu A\,\mu M^{-1}\,cm^{-2}$ and 3 nM, respectrively. The electrode is well reproducible, stable, and represents a viable platform for the analysis of DA in DA injection, human serum and rat brain sample.

Keywords: Electrocatalysis · Dopamine · Human serum · Rat brain sample · Dopamine hydrochloride injection

1 Introduction

Dopamine (DA) is a simple organic catecholamine, which plays an essential physiological role as an extracellular chemical messenger in central nervous system and cardiovascular system. The DA concentration level in biological systems is 10^{-8} M to 10^{-6} M. Any changes in the level of DA and losess of neurotransmitter in the human body cause several diseases such as Parkinson's disease, schizophrenia and attention deficit hyperactivity disorder (ADHD) [1–5]. Besides, the hydrochloride salt of DA is used in the shock treatment, which may be caused by hearth attack, open heart surgery, kidney failure and severe bacterial infections of the blood [6,7]. Therefore, the sensitive and selective detection of DA is greatly important. At present, various analytical techniques have been used for the determination of DA, such as mass spectrometry, high performance liquid chromatography, spectrophotometry, chemiluminescence and electrochemical methods. Among these methods, electrochemical methods are the preferable methods due to their simplicity, high sensitivity, fast response, and low cost. Eventhough, DA coexists with ascorbic acid (AA) in extra cellular fluids of the mammals, the concentration of AA is higher (100–1000 times) than that of DA. Genrally, the AA and uric acid (UA) are the two important interfering molecules in DA detection attributed to their similar oxidation potential [8,9]. The unmodified electrodes are unable to discriminate their voltammetric signals of DA, AA and UA. In order to solve these problems, researchers focusing to develop highly sensitive and selective transducer materials [10,11].

Graphene is a two-dimensional material composed of sp^2 bonded carbon atoms. Graphene is widely applied in diverse research areas ascribed to its outstanding properties such as large surface-to-volume ($2630\,m^2\,g^{-1}$), high electrical conductivity, chemical stability, fast adsorption kinetics, high mechanical strength, easy to surface modification, good fluorescence quenching properties and chemical inertness [12–17]. The stability arising from long range delocalisation of π-electrons giving rise to an extended aromatic network of C=C bonds across the entire basal plane [18]. Graphene can be used as a colloidal liquid lubricant due to its high chemical inertness and extreme strength. It has been widely used in various applications such as, fuel cells, supercapacitors, batteries, solar cells, field effect transistors, corrosion inhibiting coatings and so on [19–22]. Likewise, reduced graphene oxide

[a] S. Sakthinathan, S. Kubendhiran, S. M. Chen, K. Manibalan, M. Govindasamy, S. T. Huang
Electroanalysis and Bioelectrochemistry Lab
Department of Chemical Engineering and Biotechnology
National Taipei University of Technology, No. 1, Section 3
Chung-Hsiao East Road, Taipei 106, Taiwan (R.O.C)
Fax: +886227025238; Tel: +886227017147
*e-mail: smchen78@ms15.hinet.net

[b] P. Tamizhdurai
National Centre For Catalysis Research (NCCR), Indian Institute of Technology, Chennai

Supporting information for this article is available on the WWW under http://dx.doi.org/10.1002/elan.201600085.

(RGO) exhibits superior conductivity than graphene oxide (GO) and it has more active edge plane defects and larger effective surface area than GO. The electrochemical reduction method of GO to RGO is advantageous over chemical reduction methods due to its low-cost, toxic free, green and fast approach. The RGO based nanocomposites are widely known for their sensor appications [23,24].

The functionalisation of graphene via noncovalent π-π interaction with other materials such as metal porphyrins can create interesting materials [25]. The porphyrin molecules are a class of macrocyclic compounds and it is play an important role in biological organisms [26,27]. Porphyrin have rich redox properties and hence they have widespread applications in electrocatalysis [28–32]. The coordination sites of porphyrin molecule can easily connected with metal ions to form stable metal-tetraphenylporphyrins (M-TPP) [33]. The TPP metallated with Zn forms a low molecular weight complex and it is an interesting material with excellent donor unit. The Zn-TPP shows stronger binding interaction with biological analogues and decreases the hydrophobicity of the molecules. The Zn-TPP has high chemical activity and forms stable coordination bonds (stability constant of ZnTPP 10^{-29}) with pyridyl moieties. Therefore, it is more useful in different fields, such as sensors, catalysis, and energy conversion and so on [34,35]. Herein, we are interested to prepare porphyrin functionalized graphene electrode materials used for the selective detection of DA. In our research group, we continuously focus on the graphene materials functionalized with metal porphyrins and phthalocyanines. For instance, we have developed cobalt (II) phthalocyanine (CoPc) [36], cobalt phthalocyanine/iron phthalocyanine (Co-Pc)/(FePc) composites [37], iron phthalocyanine (FePc) [38], nickel tetra sulfonated phthalocyanine (NiTsPc) [39], metallated tetra phenyl porphyrin (M-TPP) like copper tetraphenylporphyrin (Cu-TPP) [40], manganese tetra phenyl porphyrin (Mn-TPP) [41], Cobalt-porphyrin-platinum functionalized reduced graphene oxide [42] and rhenium–porphyrin [43] based composites for electrochemical sensing applications. From these studies, we understood that the electron rich environment provided by such functional moieties plays a vital role in electroanalytical performance and they provide high selectivity to DA detection. The combination of RGO with Zn-TPP via non-covalent interaction might significantly increase the electrocatalytic activity. Moreover, the Zn-TPP is a good candidate for sensor applications due to the presence of Zn metal and suitable substituents [44,32].

The main objective of the present work is to prepare zinc-tetraphenylporphyrin (Zn-TPP) on RGO via non-covalent functionalization and explore it for selective and sensitive determination of DA. The flattening of metal-porphyrin molecules can further reduce distance between the metal-porphyrin and GO by electrochemical method. The RGO/Zn-TPP nanocomposite exhibited a very high electrocatalytic activity towards DA oxidation. The RGO/Zn-TPP nanocomposite shows an excellent selectivity for the electrochemical detection of DA in the nanomolar level with high sensitivity and linear range.

2 Experimental

2.1 Materials and Methods

Graphite powder (<20 μm), propionic acid, benzaldehyde, pyrrole, methanol, zinc acetate, potassium ferricyanide, potassium ferrocyanide, dopamine hydrochloride and all other chemicals were received from Sigma-Aldrich. Dopamine hydrochloride injection (easy dopa injection 1.6 mg mL^{-1}) was purchased from Chi Sheng chemical corporation, Taiwan for real sample analysis. The rat brain sample collected based on our previous report and stored in −80 °C for the real sample analysis [45]. All the chemicals, solvents, and reagents used were of analytical grade. 0.05 M phosphate buffer (pH 7) was used as supporting electrolyte which was prepared by using Na_2HPO_4 and NaH_2PO_4. Double distilled water was used to prepare all the solutions. Electrochemical measurements were carried out using CHI410 and CHI750 electrochemical workstations (Shanghai Chen Hua. Co) at room temperature. Three electrodes system consists of modified glassy carbon electrode (GCE, active area = 0.071 cm^2) as a working electrode, Ag/AgCl (saturated KCl) as a reference electrode and platinum wire as a counter electrode was used. The area of the working electrode used in amperometric experiments is 0.21 cm^2. H^1 Nuclear Magnetic Resonance (NMR) and UV-Visible spectra were recorded in JEOL 500 MHz and JASCO V770, respectively. Scanning electron microscope (SEM) performed using Hitachi S-3000H scanning electron microscope. Elemental analysis were carried out using HORIBA EMAX X-ACT (model 51-ADD0009). Electrochemical impedance spectra (EIS) were carried out using ZAHNER, Kroanch, Germany (frequency range 0.1 Hz to 1 MHz). TEM investigations were performed using JEOL 2000 transmission electron micrsope (operating at 200 Kv), wherein the sample was dripped on standard carbon/Cu grids and used for the TEM analysis. The biological sample experimental protocols were approved by the institutional animal ethic committee, Chang Gung University, Taiwan [46].

2.2 Synthesis of Zinc Tetraphenylporphyrin (Zn-TPP)

The Zn-TPP was prepared according to the previous report (Scheme 1) [47,48]. First, pyrrole (50 mL/0.8 M) and benzaldehyde (80 mL/0.8 M)) were added to reflux flask, subsequently propionic acid (500 mL) was added and the whole mixture was refluxed for 45 min. The refluxed solution was cooled to room temperature. Furthermore, the refluxing solution was filtered and washed with methanol to yield TPP (90 %). The Zn-TPP was prepared from the as-synthesized TPP. The TPP (50 mg) was dissolved in chloroform (20 mL) with following addition of

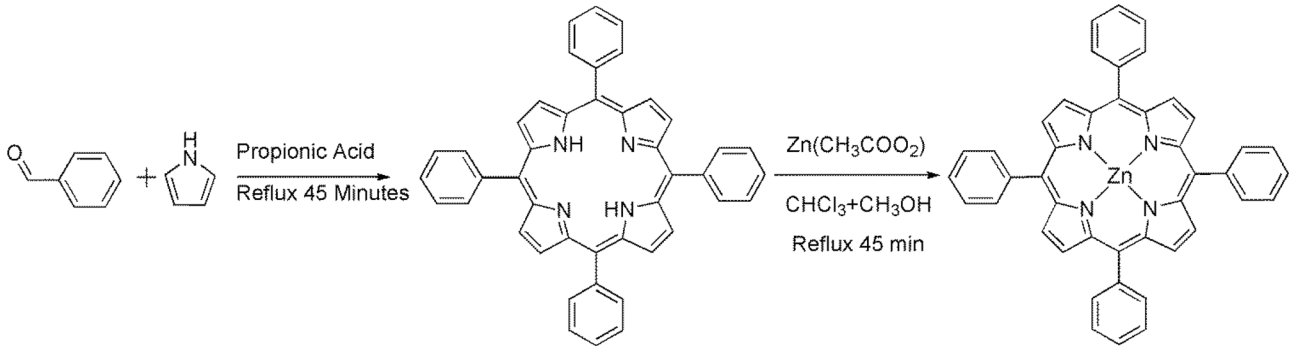

Scheme 1. Synthesis of Zinc Tetra Phenyl Porphyrin (ZnTPP).

zinc acetate (0.65 g) and methanol (5 mL). The whole mixture was refluxed for 1 h. The final reaction mixture was further washed with cooling water twice to remove unreacted materials. Finally, the Zn-TPP (88 %) was obtained after removal of solvent was chromatographed on a silica column packed with $CHCl_3$. The synthesized Zn-TPP was confirmed by NMR (Figure S1, S2).

2.3 Preparation of Reduced Graphene Oxide/Zinc Tetraphenylporphyrin (RGO/Zn-TPP) Nanocomposite

Graphene oxide (GO) was prepared from the graphite by modified Hummer's method [49]. The electrochemical preparation of RGO/Zn-TPP nanocomposite is given in scheme 2. In brief, 5 µL (1 mg mL^{-1}) dispersion of Zn-TPP was dropped into GO (2 mg mL^{-1}) solution and the resulting mixture was treated by ultrasonication for 20 min in order to attain complete interaction between Zn-TPP and GO. Subsequently, the GO/Zn-TPP dispersion was filtered and washed with absolute ethanol for 3 times, then dried at 70 °C. Then, GO/Zn-TPP (2 mg mL^{-1}) was dispersed in DMF through ultrasonication for 30 min. About 8 µL of GO/Zn-TPP suspended solution was drop coated on the well-polished GCE surface and then dried at room temperature. 8 µL of GO/Zn-TPP delivered maximum catalytic reponse to DA (Figure S3). Furthermore, the GO/Zn-TPP/GCE was transferred into electrochemical cell containing 0.05 M acetate buffer and electrochemical reduction was carried out. The applied potential range was 0 to −1.30 V with 20 cycles (Figure S4). Then, the RGO/Zn-TPP nanocomposite modified electrode was used for the oxidation of DA in deoxygenated phosphate buffer (pH 7).

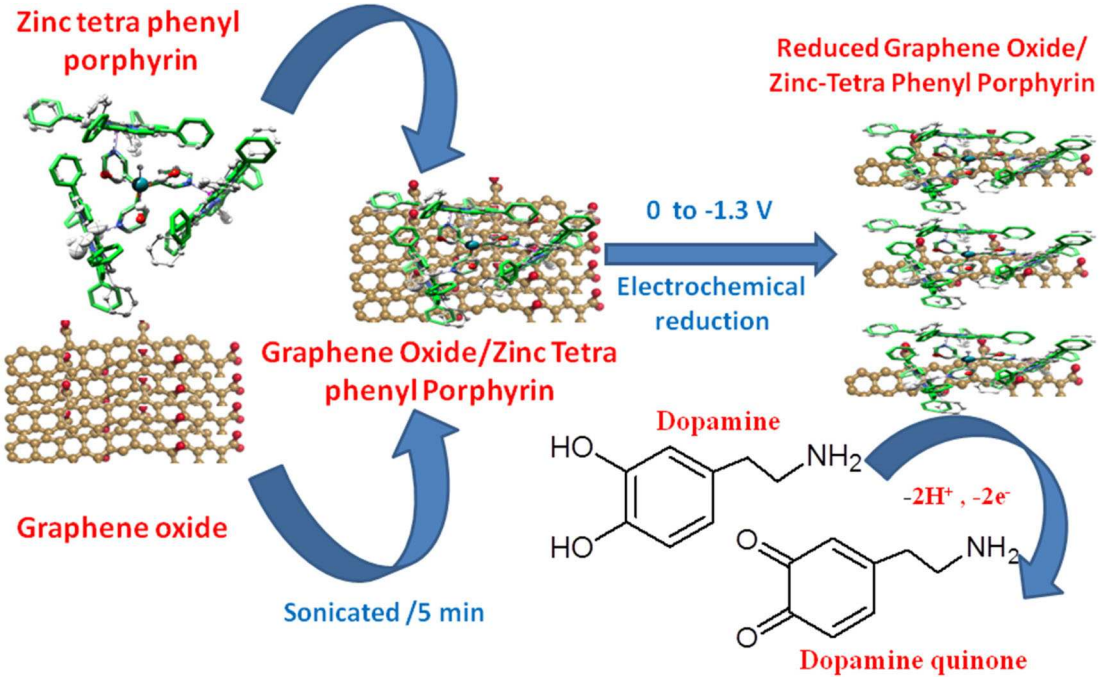

Scheme 2. Schematic representation for the preparation of RGO/Zn-TPP nanocomposite

3 Results and Discussion

3.1 Materials Characterization

Figure 1 shows the SEM images of GO (A), GO/Zn-TPP (B), RGO/Zn-TPP (C), and Zn-TPP (A′). The morphological structure of GO (Figure 1A) presents multiple sheets with randomly arranged surfaces. The SEM image of GO/Zn-TPP (Figure 1B) exhibited the wrinkled structure of surface morphology. The RGO/Zn-TPP nanocomposite (Figure 1C) showed well exfoliated and thin crumbled sheets closely associated with each other. The average sheet thickness is found to be around 63 nm. Figures 1D and D′ display the EDX spectrum of RGO/Zn-TPP nanocomposite, which confirms the presence of C, O and Zn atoms in the composite. Figure D′ shows the quantitative EDX results based on the mass fraction of carbon. The elemental analysis was revealed the presence of Zn-TPP molecule on the RGO surface. Figure 2 shows the TEM images of RGO (A), Zn-TPP (B) and RGO/Zn-TPP (C, D). Figure 2A showed typical, wrinkled and folding sheet like structure of RGO. Figure 2B shows the uniformly distributed small ball like Zn-TPP molecule. Besides, the TEM image of Figure 2C and 2D shows the morphology of RGO/Zn-TPP nanocomposite in which the Zn-TPP molecules were randomly arranged onto the RGO sheets surface.

The electrochemical impedance spectroscopy analysis (EIS) is an efficient tool for studying the electron transfer resistance at the modified electrode. The Nyquist plot shows two kinds of region; first region is for electron transfer resistance (R_{et}) and second linear region is for diffusion process. Figure 3A shows the EIS spectrum of (a) bare GCE, (b) GO, (c) GO/Zn-TPP, (d) RGO, (e) RGO/Zn-TPP and (a′) Zn-TPP modified electrode in 5 mM $[FeCN_6]^{3-/4-}$ solution containing 0.05 M phosphate buffer (pH 7) with 0.1 M KCl electrolyte. The frequency range was from 0.1 Hz to 1 MHz. The R_{ct} values of the

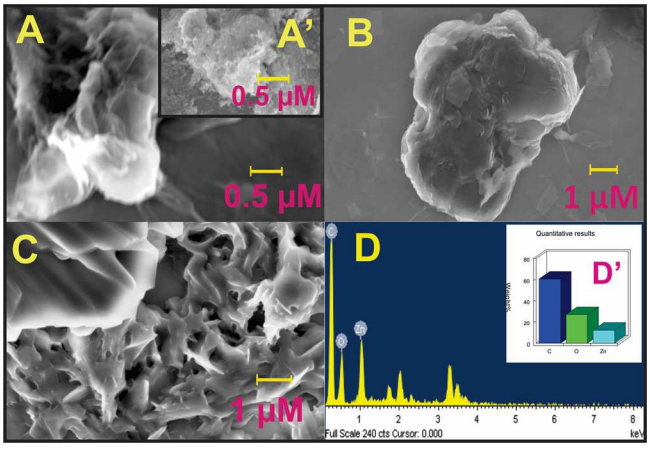

Fig. 1. SEM images of (A) GO, (A′) Zn-TPP, (B) GO/Zn-TPP and (C) RGO/Zn-TPP nanocomposite. (D) and (D′) EDX spectrum and Elemental composition of RGO/Zn-TPP nanocomposite.

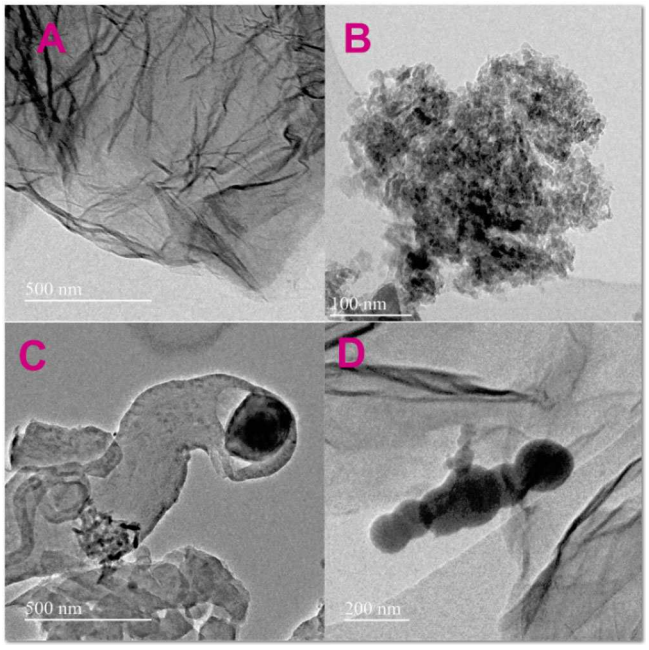

Fig. 2. TEM images of (A) RGO, (B) Zn-TPP, (C, D) RGO/Zn-TPP nanocomposite.

electrodes were obtained by fitting the Nyquist plot results with Randles equivalent circuit model (Table S3). The bare GCE shows large semicircle with R_{ct} of 604 Ω. After the modification of GCE with GO, the R_{ct} value was decreased to 480 Ω,. Similarly, the R_{ct} values of RGO and GO/Zn-TPP modified electrodes were estimated to be 340 Ω and 280 Ω respectively. The inset of Fig. 3A shows the EIS spectrum of Zn-TPP modified electrode which exhibits larger semicircle than that of the other modified electrodes due to the poor conductivity of Zn-TPP. Interestingly, the RGO/Zn-TPP nanocomposite modified electrode showed small R_{ct} of 152 Ω which is lower than all the other modified electrodes. Because, the RGO and ZnTPP make a strong π-π noncovalent interaction, the electrical conductivity greatly enhanced over control electrodes.

Figure 3B shows the UV-Visible spectra of (a) Zn-TPP, (b) RGO/Zn-TPP, (c, c′) GO, (d, d′) RGO. The absorption bands (Q bands) responsible for the red to purple color are observed in the visible region between 500 to 700 nm for free porphyrin. A Soret band was appeared around 400 nm in the near UV region for metalated prophyrin [50]. Soret band is an intense peak in the blue wavelength region of the visible spectrum. The Zn-TPP shows very shorp absorption peak appeared at 419 nm and also shows some weaker absorption peaks (548 nm, 582 nm) for Q-band due to the π-interaction. The RGO/Zn-TPP shows decreases in the intensity of Soret and Q-bands at 415 nm and 532, 610 nm. This is ascribed to the strong π-π non-covalent interaction between Zn-TPP and RGO. Thus, the insertion of TPP in RGO was confirmed by the decrease in Soret band [51] and reduction in number of Q-bands as compared to Zn-TPP and RGO.

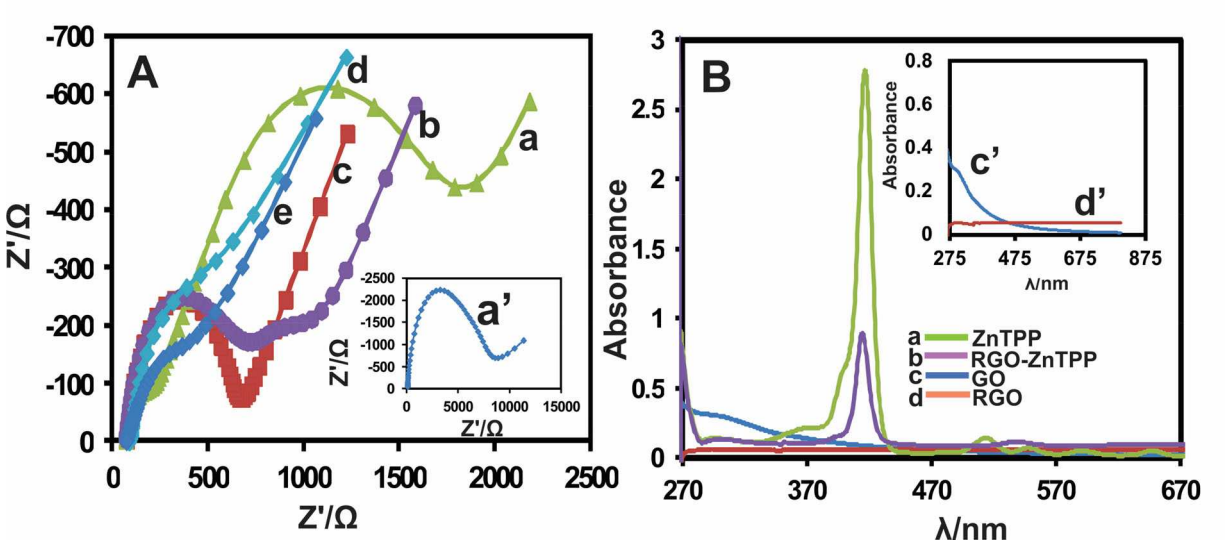

Fig. 3. **A**) Electrochemical Impedance spectra of (a) GO, (b) GO/Zn-TPP, (c) Bare GC, (d) RGO, (e) RGO/Zn-TPP and (a′) Zn-TPP modified electrode in 0.05 M phosphate buffer (pH 7) containing the mixture solution 5 mM $[Fe(CN)_6]^{4-/3-}$ and 0.1 M KCl. **B**) UV-Vis spectroscopy analysis of (a) Zn-TPP, (b) RGO/Zn-TPP (c, c′) RGO, (d, d′) GO.

The metalation was observed that there is a red shifting in the Soret band. Therefore, the number of absorption bands observed is less than free TPP. The insert to Figure 2B depicts the UV-Vis spectra of GO and RGO. The absorbance of GO and RGO showed typical bands at 224 nm and 282 nm due to the π-interaction and by the reduction of GO, respectively.

3.2 Electrocatalytic Behavior of DA at Different Modified Electrodes

Figure 4A shows the CVs obtained at (b) GCE, (c) GO/GCE, (d) GO/Zn-TPP/GCE, (e) RGO/GCE and (f) RGO/Zn-TPP in phosphate buffer (pH 7) containing 200 μM DA. The curve (a) in Figure 4A shows CV obtained at RGO/Zn-TPP/GCE in absence of DA. The bare GCE shows the DA oxidation peak potential (E_p) at 0.251 V and anodic peak current (I_{pa}) at 4.611 μA. At GO/GCE, the E_{pa} and I_{pa} were obtained as 0.208 V and 6.309 μA respectively. At RGO/GCE, the E_p and I_{pa} were obtained as −0.239 V and 4.445 μA. Here, the oxidation peak current shifted to negative side indicating reduction in overpotential. The GO/Zn-TPP modified electrode showed improved performance with E_{pa} at 0.210 V and I_{pa} at 10.95 μA. In comparion with control electrodes, RGO/Zn-TPP/GCE showed significantly improved catalytic performances with E_{pa} of 0.214 V and I_{pa} of 45.97 μA (Table S1). The RGO/Zn-TPP nanocomposite modified electrode showed excellent electrocatalytic activity to DA with significantly enhanced current response than the control electrodes. Inset Figure 4B shows the error bar, relative standard deviation of three measurements.

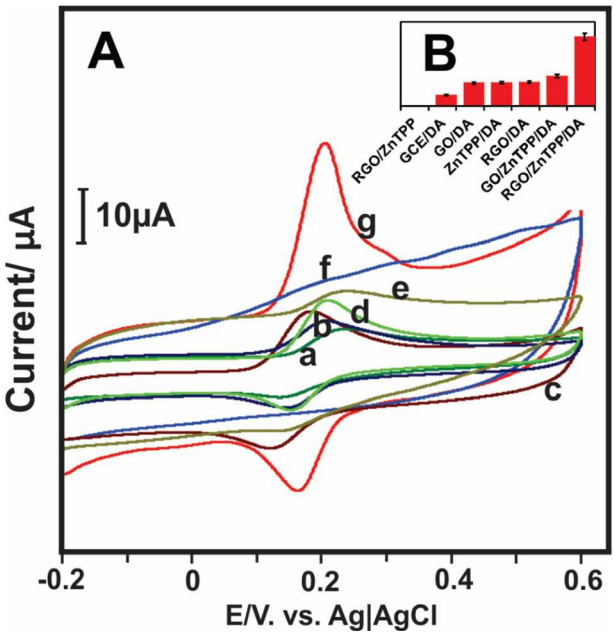

Fig. 4. **A**) Cyclic voltammograms of (b) GCE, (c) GO/GCE, (d) GO/Zn-TPP/GCE, (e) RGO/GCE and (f) RGO/Zn-TPP in phosphate buffer (pH 7) containing 200 μM DA. The curve (a) shows CV obtained at RGO/Zn-TPP/GCE in absence of DA. **B**) Inset shows the peak current vs. different film, the error bars relative to the standard deviation of 3 measurements.

3.3 Effect of Scan Rate and pH

The effect of scan rate was evaluated by CVs at RGO/Zn-TPP nanocomposite modified electrode in 0.05 M phosphate buffer containing 200 μM DA at the scan rate ranges from 10–100 mV s^{-1} (Figure 5A). The anodic and cathodic peak currents increased as the scan rate increas-

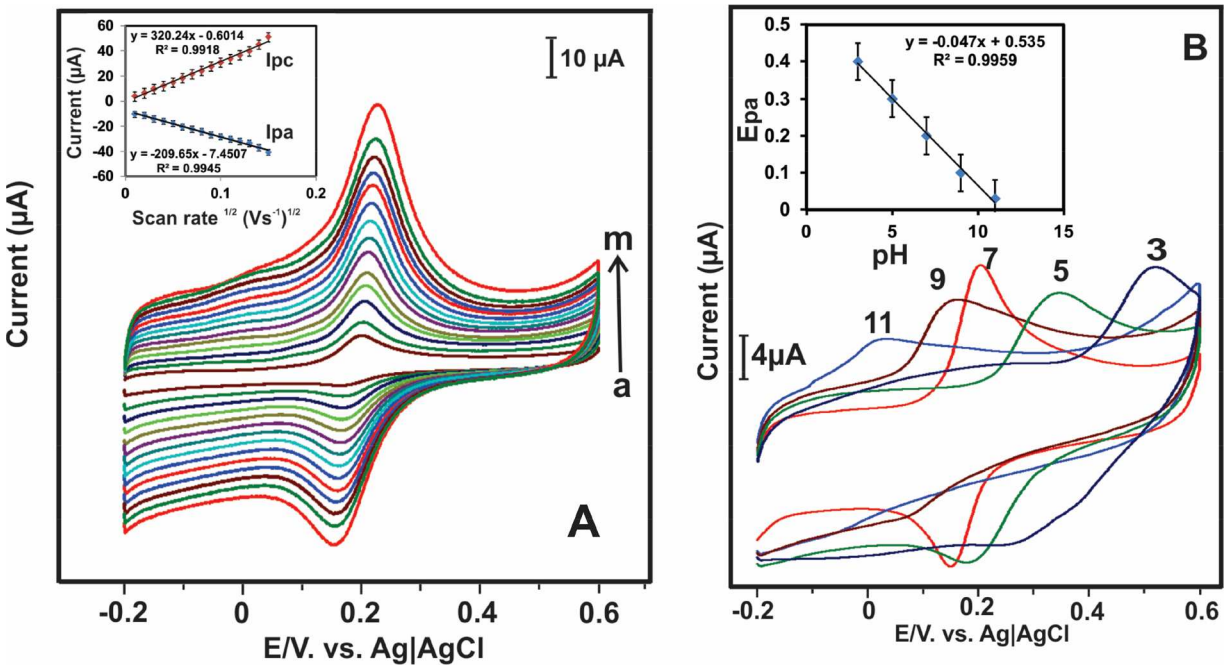

Fig. 5. **A**) Cyclic voltammetry response of the modified RGO/Zn-TPP nanocomposite modified GCE in phosphate buffer (pH 7) containing 200 μM of DA at different scan rate (10–100 mV s^{-1}; a–m). Insert, calibration plot of scan rate vs. peak current. **B**) Cyclic voltammetry response of RGO/Zn-TPP nanocomposite modified GCE in phosphate buffer (pH 7) 200 μM DA containing different pH solution (3, 5, 7, 9, and 11) at the scan rate of 50 mV s^{-1}. Insert shows the calibration plot for pH vs. E^0.

es. The inset to Figure 4A shows the plot of I_{pa} and I_{pc} vs. square root of scan rate. Both I_{pa} and I_{pc} were linearly increased by increasing the scan rate. This result indicated that the oxidation process of DA at RGO/Zn-TPP nanocomposite film modified electrode is a diffusion controlled process. Figure 5B shows the electrocatalytic performance of RGO/ZnTPP nanocomposite modified electrode in various pH (3 to 11) PBS, containing 200 μM DA at the scan rate 50 mV s^{-1}. The catalytic peak current increases from low pH to high pH. The response current reached maximum at pH 7.0, but after that it started to decrease gradually. Therefore, pH 7.0 was chosen for all analytical experiments. The insert Figure 5B shows linear dependence between the anodic peak potential (E_p) and different pH. The slope value is almost close to the Nernst equation (−59 pH/mV). This result shows that the oxidation of DA at RGO/Zn-TPP electrode involves equal numbers of proton and electrons. The corresponding oxidation mechanisms is proposed in Scheme 3. Moreover, the electrochemical oxidation of dopamine is an ECE mechanism (Where E and C denoted electrochemical and chemical steps, respectively) [52,53]. The electrochemically active surface area of the electrodes can be estimated using $K_3[Fe(CN)_6]$ as a model complex and by following Randles Sevcik equation. The active surface area of RGO/Zn-TPP (0.186 cm^2) is significantly higher than that of GO/Zn-TPP (0.156 cm^2), RGO (0.121 cm^2) and GO (0.118 cm^2) electrodes (Table S2) [54,55].

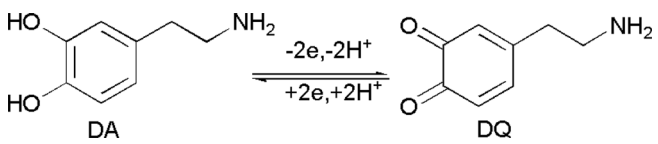

Scheme 3. Electrochemical oxidation of Dopamine (DA)

3.4 Amperometric Determination of DA

Amperometric method is more sensitive method than that of the cyclic voltammetry method. It has been widely used for the analysis of low analytes concentration. The RGO/Zn-TPP modified electrode towards DA was investigated by the amperometric method. The applied potential is 0.20 V. Figure 6A shows the amperometric performance of RGO/Zn-TPP/GCE for different concentrations of DA into the deoxygenated phosphate buffer (pH 7). The RGO/Zn-TPP nanocomposite did not show any response in the absence of DA, whereas well-defined responses were observed for each addition of DA. The DA molecule loses of two electrons to form dopamine quinone. Then, the reduced Zn-TPP interacts with the positively charged DA molecule. The oxidation peak current increases linearly (0.05–238.8 μM) with increasing concentration of DA. Figure 6A inset shows the linear relationship between DA and peak current. The detection limit was calculated to be 3 nM (S/N = 3) and the sensitivity was estimated to be 0.665 μA μM^{-1} cm^{-2}. The analytical performance of the RGO/Zn-TPP nanocomposite was compared with previously reported modified electrode and given as Table 1. The results are comparable with previous reports and hence the RGO/Zn-TPP nanocom-

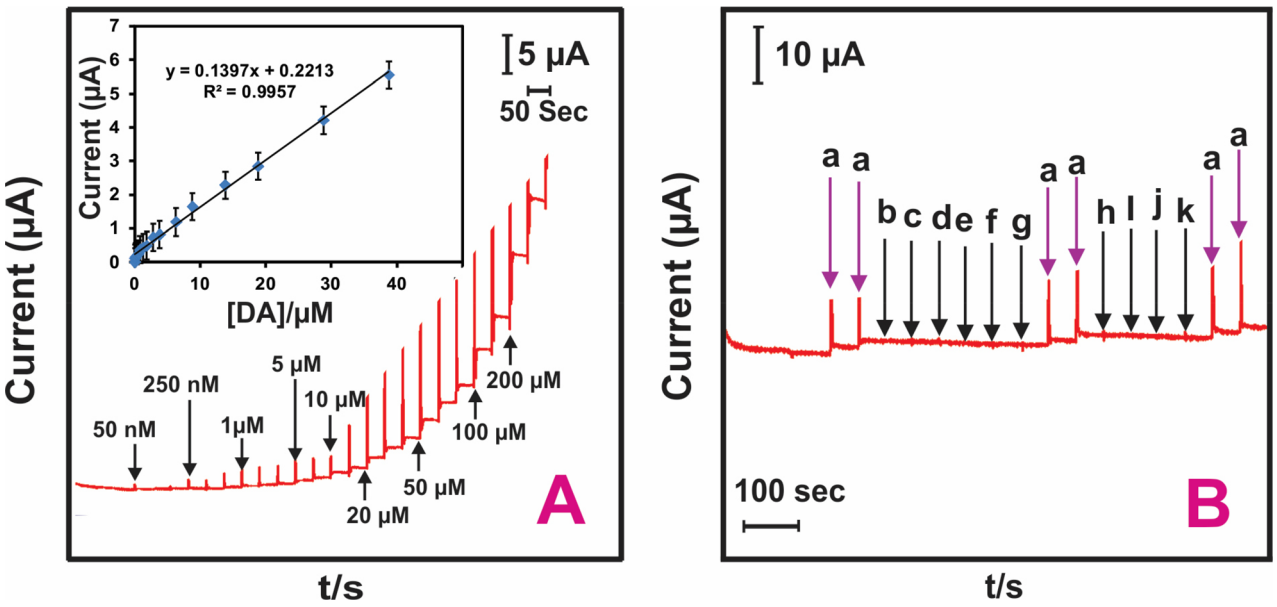

Fig. 6. (**A**) Amperometric response for the oxidation DA with different concentration in phosphate buffer (pH 7), E_{app} = 0.2 V. Insert shows the plot of peak current vs. DA concentration. (**B**) Amperometric response of DA at RGO/Zn-TPP in presence of interfering molecule, E_{app} = 0.2 V.

Table 1. Comparison of analytical performance of RGO/Zn-TPP with other reports for the detection of dopamine

Electrode materials	Linear range (μM)	LOD [a]	Ref.
GNS [b] /BiNPs [c]	1–30	0.35 μM	[58]
β-CD [d]/Graphene/GCE	0.9–200	5.0 nM	[59]
PPy [e]/ Graphene/GCE	0.5–10.0	0.1 μM	[60]
Graphene/AuNPs [f]/GCE	0.1–10	0.04 μM	[26]
rGO [g]/GCE	0.1–10	0.1 μM	[61]
Graphene oxide/GCE [h]	1–15	0.27 μM	[62]
Graphene/Pt-PANI[p]	1–100	0.6 μM	[6]
Graphene nanosheet	2–1000	0.85 μM	[9]
Porphyrin/Graphene/GCE	1–7	9.45 nM	[32]
MWCNT [i]/Graphene oxide/GCE	0.5–400	60 nM	[63]
Graphene/Chitosan/GCE	0.2–100	9.82 nM	[64]
AuNPs/Graphene oxide/GCE	0.1–10	0.05 μM	[65]
Graphene/Pd [j]-PtNPs [k]/GCE	4–400	0.04 μM	[66]
Graphene/PtNPs/GCE	0.03–8.13	0.03 μM	[67]
Pyrolytic carbon film/GCE	18–270	2.3 μM	[68]
CRGO [l]/CuTPP [m]/GCE	2–200	0.76 μM	[40]
RGO/MnTPP [n]/GCE	0.3–188.8	8 nM	[41]
RGO/Zn-TPP [o]/GCE	0.04–238.8	3 nM	This work

Abbreviations: [a] LOD – Limit of detection, [b] GND – Graphene nanosheet, [c] Bismuth nanoparticles, [d] β-CD – β-Cyclodextrin, [e] PPy – Poly pyrrole, [f] AuNPs – Gold nanoparticles, [g] rGO – Reduced graphene oxide, [h] GCE – Glassy carbon electrode, [i] MWCNT – Multiwalled carbon nanotube, [j] PdNPs – Palladium nanoparticles, [k] PtNPs – Platinum nanoparticles, [l] Chemically reduced graphene oxide, [m] Copper tetraphenylporphyrin, [n] Manganese tetraphenylporphyrin, [o] Zn-TPP – Zinc tetraphenylporphyrin. [P]PANI-polyaniline.

posite modified electrode has the potential electrode materials for DA detection.

3.5 Selectivity, Reproducibility and Repeatability

Figure 6B shows the selectivity of RGO/Zn-TPP nanocomposite film modified electrode towards detection of DA in presence of common interfering molecules. The operating potential of the electrode was held at +0.20 V and the rotation speed was 1500 RPM. The modified electrode exhibited well defined amperometric response for the addition of 5 μM DA (a). However, there is no noteworthy peak appeared for the addition of 500 μM interfering molecules, such as ascorbic acid (b), uric acid (c), glycine (d), glucose (e), lysine (f), fructose (g), maltose (h), citric acid (i), epinephrine (j), and norepinephrine (k). Interestingly, notable amperometric response was observed for the addition of 5 μM DA in to the same phos-

phate buffer containing the above interfering molecules. The selectivity study is also carried out using cyclic voltammetry which showed similar results as amperometry (Figure S5). Therefore, the RGO/Zn-TPP nanocomposite modified electrode has good selectivity of DA detection even in the presence of 100 fold excess concentration of interfering molecules. This is due to the electrostactic attractive interaction between positive charged DA and negative charged RGO/ZnTPP. On the other hand, interference species were repuled due to the electrostatic repulsion [56,57]. It is a good evidence for the selectivity of RGO/Zn-TPP nanocomposite modified electrode for DA detection. The stability studies were carried out in phosphate buffer containing 5 μM DA. The prepared RGO/Zn-TPP nanocomposite electrode was prepared and stored in refrigerator for 15 days. Every day, the catalytic response of the electrode is measured. The prepared sensor only lost 4% from the initial sensitivity after 15 days of storage which indicates good stability of the electrode. To identify reproducibility of the modified electrode, the three different modified electrodes were prepared. Here, the relative standard deviation (RSD) of the three electrodes was found to be 2.6%. Similarly, the modified electrode showed good repeatability with RSD of 3.5% (for 3 repeatable measurements). Thus, the modifed electrode exhibited satisfactory repeatability, reproducibility and stability. The practical feasibility of the proposed sensor was analyzed by the determination of DA in dopamine hydrochloride injection, Human serum and rat brain sample. Standard addition method was used for the analysis of DA from the real sample analysis. Human serum sample was obtained from Local hospital Taiwan, and rat brain sample collected from rat based on previous report. The real samples (dopamine hydrochloride injection, human blood serum and rat brain sample) were spiked with phosphate buffer (pH 7) and the recovery values were calculated and listed in Table 2, 3, and 4 (Fig. S6). The average recovery values obtained for dopamine hydrochloride injection, Human serum and rat brain sample were of 90.95%, 92.05%, and 93.35% respectively. The acceptable recoveries obtained in real sample studies revealed good practicality of the developed modified electrode.

4 Conclusions

In summary, the RGO/Zn-TPP nanocomposite was successfully prepared through easily adoptable electrochemical method. The SEM, UV-Vis, and NMR spectroscopy methods were used to characterize the nanocomposite. The CV and an amperometry method (*i*-t) were used to measure the electrocatalytic activity of RGO/Zn-TPP towards DA oxidation. The prepared RGO/Zn-TPP nanocomposite shows enhanced electrocatalytic activity at the potential of 0.214 V (vs. Ag/AgCl) and showed wide linear range (0.04 to 238.8 μM). The electrode sensitivity is 0.665 $\mu A\,\mu M^{-1}\,cm^{-2}$ and the detection limit is 3 nM. Moreover, the prepared sensor shows good reproducibility, repeatability, and stability. The developed sensor showed excellent practical feasibility in rat brain blood, serum and dopamine injection sample. The RGO/Zn-TPP composite has great potential in electrochemical sensing applications.

Table 2. Determination of DA in DA hydrochloride injection using RGO/Zn-TPP nanocomposite modified GC electrode.

DA Samples	Added (μM)	Found [a] (μM)	Recovery (%)	RSD [b] (%)
1	–	2.3	–	–
2	2.0	3.8	88.3	3.8
3	2.0	5.9	93.6	3.7

1, 2 and 3 diluted DA hydrochloride injection sample, [a] Standard deviation, [b] Relative standard deviation of this measurement is (n = 3).

Table 3. Determination of DA in Human serum sample using RGO/Zn-TPP nanocomposite modified GC electrode.

Human serum sample	Added(μM)	Found [a] (μM)	Recovery (%)	RSD [b] (%)
1	–	1.5	–	–
2	2.0	3.2	91.4	3.4
3	2.0	5.1	92.7	3.8

1, 2, and 3, diluted Human serum sample, [a] Standard deviation, [b] Relative standard deviation for three measurements.

Table 4. Determination of DA in Rate brain serum sample using RGO/Zn-TPP nanocomposite modified GC electrode.

Rat brain sample	Added(μM)	Found [a] (μM)	Recovery (%)	RSD [b] (%)
1	–	0.4	–	–
2	2.0	2.3	95.8	3.6
3	2.0	4.0	90.9	3.8

1, 2, and 3, diluted Rat brain serum sample, [a] Standard deviation, [b] Relative standard deviation for three measurements.

Acknowledgements

This work was supported by the National Science Council and the Ministry of Education, Taiwan (ROC) and Indian Institute of Technology, Chennai, India, for TEM characterization.

References

[1] A. Pandikumar, G. T. S. How, T. P. See, F. S. Omar, S. Jayabal, K. Z. Kamali, N. Yusoff, A. Jamil, R. Ramaraj, S. A. John, H. N. Lim, N. M. Huang, *RSC Adv.* **2014**, *4*, 63296–63323.
[2] S. Hong, L. Y. S. Lee, M. H. So, K. Y. Wong, *Electroanalysis* **2013**, *4*, 1085–1094.
[3] R. K. Shervedani, M. Bagherzadeh, S. A. Mozaffari, *Sensors and Actuators B.* **2006**, *115*, 614–621.
[4] R. K. Shervedani, S. M. S. Barzoki, M. Bagherzadeh, *Electroanalysis* **2010**, *22*, 969–977.
[5] L. N. Wu, Y. L. Tan, L. Wang, S. N. Sun, Z. Y. Qu, J. M. Zhang, Y. J. Fan, *Microchim. Acta.* **2015**, *182*, 1361–1369.
[6] M. Bagherzadeh, S. A. Mozaffarib, M. Momeni, *Anal. Methods.* **2015**, *7*, 9317–9323.
[7] Z. Guo, M. L. Seol, M. S. Kim, J. H. Ahn, Y. K. Choi, J. H. Liub, X. J. Huang, *Analyst.* **2013**, *138*, 2683–2690.
[8] C. Karuppiah, R. Devasenathipathy, S. M. Chen, D. Arulraj, S. Palanisamy, V. Mani, V. S. Vasantha, *Electroanalysis* **2015**, *27*, 485–493.
[9] M. Bherzadeh, M. Heydari, *Analyst.* **2013**, *138*, 6044–6051.
[10] M. S. Hsu, Y. L. Chen, C. Y. Lee, H. T. Chiu, *ACS Appl. Mater. Interfaces.* **2012**, *4*, 5570–5575.
[11] S. Palanisamy, B. Thirumalraj, S. M. Chen, A. Ali, F. M. A. A. Hemaid, *J. Colloid. Inter. Sci.* **2015**, *448*, 251–256.
[12] G. Fabregat, E. Armelin, C. Aleman, *J. Phys. Chem. B.* **2014**, *118*, 4669–4682.
[13] Y. Liu, Y. Xia, H. Yang, Y. Zhang, M. Zhao, G. Pan, *Nanotechnology.* **2013**, *24*, 235401–235408.
[14] A. Yang, Y. Xue, H. Zhao, X. Li, Z. Yuan, *Microchim. Acta.* **2015**, *182*, 341–349.
[15] L. Cui, T. Pu, Y. Liu, X. He, *Electrochim. Acta.* **2013**, *88*, 559–564.
[16] L. Wang, Y. Ye, X. Lu, Z. Wen, Z. Li, H. Hou, Y. Song, *Sci. Rep.* **2013**, *3*, 3568–3576.
[17] B. J. Sanghavi, O. S. Wolfbeis, T. Hirsch, N. S. Swami, *Microchim. Acta.* **2015**, *182*, 1–41.
[18] L. Kyh, S. F. Nielsen, A. G. Cabo, A. Cassidy, J. A. Miwab, L. Hornekaer, *Faraday Discuss.* **2015**, *180*, 495–509.
[19] X. Xu, D. Huang, K. Cao, M. Wang, S. M. Zakeeruddin, M. Gratzel *Sci. Rep.* **2013**, *3*, 1489–1495.
[20] K. Xu, X. Meshik, B. M. Nichols, E. Zakar, M. Dutta, M. A. Stroscio, *Nanotechnology* **2014**, *25*, 205501–205509.
[21] D. Prasai, J. C. Tuberquia, R. R. Harl, G. K. Jennings, K. I. Bolotin, *Acs. nano.* **2012**, *2*, 1102–1108.
[22] D. Berman, A. Erdemir, A. V. Sumant, *Materials Today* **2014**, *17*, 31–42.
[23] J. L. Chen, X. P. Yan, K. Meng, S. F. Wang, *Anal. Chem.* **2011**, *83*, 8787–8793.
[24] H. F. Ma, T. T. Chen, Y. Luo, F. Y. Kong, D. H. Fan, H. L. Fang, W. Wang, *Microchim. Acta.* **2015**, *182*, 2001–2007.
[25] M. Bagherzadeh, A. Farahbakhsh, Surface functionalization of Graphene in Graphene Materials: Fundamental and Emerging Applications (Edited by A. Tiwari, M. Syvajarvi) Wiley, USA, **2015**, pp. 25–58.
[26] S. J. Li, D. H. Deng, Q. Shi, S. R. Liu, *Microchim. Acta.* **2012**, *177*, 325–331.
[27] L. Wu, L. Feng, J. Ren, X. Qu, *Biosens. Bioelectron.* **2012**, *34*, 57–62.
[28] L. Zheng, D. Ye, L. Xiong, J. Xu, K. Tao, Z. Zou, D. Huang, X. Kang, S. Yang, J. Xia, *Anal. Chim. Acta.* **2013**, *768*, 69–75.
[29] A. Takai, C. P. Gros, J. M. Barbe, R. Guilard, S. Fukuzumi, *Chem. Eur. J.* **2009**, *15*, 3110–3122.
[30] V. Sgobba, G. Giancane, S. Conoci, S. Casilli, G. Ricciardi, D. M. Guldi, M. Prato, L. Valli, *J. Am. Chem. Soc.* **2007**, *129*, 3148–3156.
[31] M. Calvete, G. Y. Yang, M. Hanack, *Synth. Met.* **2004**, *141*, 231–243.
[32] M. Lv, T. Mei, C. Zhang, X. Wang, *RSC Adv.* **2014**, *4*, 9261–9270.
[33] A. Charisiadis, C. Stangel, V. Nikolaou, M. S. Roy, G. D. Sharmac, A. G. Coutsolelos, *RSC Adv.* **2015**, *5*, 88508–88519.
[34] Arramel, A. C. Gomez, B. J. V. Wees, *Graphene* **2013**, *2*, 102–108.
[35] Z. Zhanga, J. Zhua, Q. Hana, H. Cui, H. Bi, X. Wanga, *Appl. Surf. Sci.* **2014**, *321,* 404–411.
[36] V. Mani, R. Devasenathipathy, S. M. Chen, S. T. Huang, V. S. Vasantha, *Enzyme Microb. Technol.* **2014**, *66*, 60–66.
[37] V. Mani, R. Devasenathipathy, S. M. Chen, J. A. Gu, S. T. Huang, *Renewable Energy* **2015**, *74*, 867–874.
[38] V. Mani, A. T. E. Vilian, S. M. Chen, *Int. J. Electrochem. Sci.* **2012**, *7*, 12774–12785.
[39] C. Karuppiah, R. Devasenathipathy, S. M. Chen, D. Arulraj, S. Palanisamy, V. Mani, V. S. Vasantha, *Electroanalysis* **2015**, 27485–493.
[40] C. Karuppiah, S. Sakthinathan, S. M. Chen, K. Manibalan, S. M. Chen, S. T. Huang, *Appl. Organometal. Chem.* **2016**, 3040–46.
[41] S. Sakthinathan, H. F. Lee, S. M. Chen, P. Tamildurai, *J. Colloid. Interface Sci.* **2016**, *468*, 120–127.
[42] J. Shu, Z. Qiu, Q. Wei, J. Zhuang, D. Tang, *Sci. Rep.*, 5: 15113, DOi: 10.1038/srep15113.
[43] C. D. Windle, M. W. George, R. N. Perutz, P. A. Summers, X. Z. Sun, A. C. Whitwood, *Chem. Sci.* **2015**, *6*, 6847–6864.
[44] G. D. Bajju, S. Kundan, M. Bhagat, D. Gupta, A. Kapahi, G. Devi, *Bioinorg. Chem. Appl.* **2014**, *13*, 2014, http://dx.doi.org/10.1155/2014/782762
[45] D. Milatovic, M. Aschner, *Curr Protoc Toxicol.* **2009**, *39*, http://dx.doi.org/10.1002/0471140856.tx1214s39.
[46] B. S. Lou, P. S. Wu, C. W. Hou, F. Cheng, J. K. Chen, *J. Pharm. Biomed. Anal.* **2014**, *94*, 99–105
[47] A. D. Adler, F. R. Longo, J. D. Finarelli, J. Goldmacher, J. Assour, L. Korsakoff, *J. Org. Chem.* **1967**, *32*, 476–476.
[48] X. Gong, T. Milic, C. Xu, J. D. Batteas, *J. Am. Chem. Soc.* **2002**, *124*, 14290–14291.
[49] W. S. Hummers, R. E. Offeman, *J. Am. Chem. Soc.* **1958**, *80*, 1339.
[50] H. Chiniforoshan, N. Safari, J. M. Nezhad, H. Hadadzadeh, A. H. Mahmoudkhani, *Inorganica Chimica Acta.* **2006**, *359*, 2101–2106.
[51] K. M. Smith, Porphyrin and metalloporphyrin, 1st edn. *Elsevier,* Amsterdam, **1975**, pp. 157–221. ISBN 0-444-41375-8
[52] E. Laviron , *J. Electroanal. Chem.* **1979**, *101*, 19–28.
[53] T. Luczak, *Electroanalysis* **2008**, *20*, 1639–1646.
[54] K. Y. Hwa, B. Subramani, *Biosensors and Bioelectronics* **2014**, *62*, 127–133.
[55] C. Liu, H. Zhang, Y. Tang, S. Luo, *J. Mater. Chem. A.* **2014**, *2*, 4580–4587.

[56] L. X. Chen, J. N. Zheng, A. J. Wang, L. J. Wu, J. R. Chen, J. J. Feng, *Analyst.* **2015**, *140*, 3183–3192.
[57] T. Q. Xu, Q. L. Zhang, J. N. Zheng, Z. Y. Lv, J. Wei, A. J. Wang, J. J. Feng, *Electrochimica Acta.* **2014**, *115*, 109–115.
[58] V. Mani, R. Devasenathipathy, S. M. Chen, K. Kohilarani, R. Ramachandran, *Int. J. Electrochem. Sci.* **2015**, *10*, 1199–1207.
[59] L. Tan, K. G. Zhou, Y. H. Zhang, H. X. Wang, X. D. Wang, Y. F. Guo, H. L. Zhang, *Electrochem. Commun.* **2010**, *12*, 557–560.
[60] Z. Zhuang, J. Li, R. Xu, D. Xiao, *Int. J. Electrochem. Sci.* **2011**, *6*, 2149–2161.
[61] X. Yu, K. Sheng, G. Shi, *Analyst.* **2014**, *139*, 4525–4531.
[62] F. Gao, X. Cai, X. Wang, C. Gao, S. Liu, F. Gao, Q. Wang, *Sensors Actuators B.* **2013**, *186*, 380–387.
[63] H. Yang, Y. Li, Y. Liu, Y. Zhang, Y. Zhao, M. Zhao, *J. Solid. State Electrochem.* **2015**, *19*, 145–152.
[64] C. Liu, J. Zhang, E. Yifeng, J. Yue, L. Chen, D. Li, *Electron. J. Biotechn.* **2014**, *17*, 183–188.
[65] W. Zhu, T. Chen, X. Ma, H. Ma, S. Chen, *Colloids. Surf B.* **2013**, *111*, 321–326.
[66] J. Yan, S. Liu, Z. Zhang, G. He, P. Zhou, H. Liang, L. Tian, X. Zhou, H. Jiang, *Colloids. Surf B.* **2013**, *111*, 392–397
[67] C. L. Sun, H. H. Lee, J. M. Yang, C. C. Wu, *Biosens. Bioelectron.* **2011**, *26*, 3450–3455.
[68] G. P. Keeley, N. Mcevoy, H. Nolan, S. Kumar, E. Rezvani, M. Holzinger, S. A. Cosniera, G. S. Duesbergbc, *Anal. Methods* **2012**, *4*, 2048–2053.

Received: February 11, 2016
Accepted: March 29, 1016
Published online: ■■ ■■, 0000

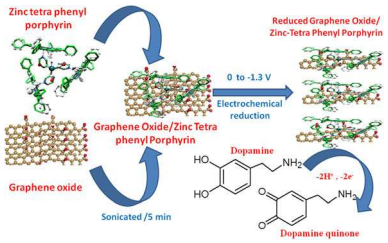

S. Sakthinathan, S. Kubendhiran, S. M. Chen, K. Manibalan, M. Govindasamy, P. Tamizhdurai, S. T. Huang**

■■ – ■■

Reduced Graphene Oxide Non-covalent Functionalized with Zinc Tetra Phenyl Porphyrin Nanocomposite for Electrochemical Detection of Dopamine in Human Serum and Rat Brain Samples